THE JOURNAL OF PHYSICAL CHEMISTRY C

Article

pubs.acs.org/JPCC

Hydrogen Abstraction Energies and Ammonia Binding to BEA, ZSM-5, and α-Quartz Doped with Al, Sc, B, or Ga

Vishal Agarwal and Horia Metiu*

Department of Chemistry and Biochemistry, University of California, Santa Barbara, California 93106-9510 United States

Supporting Information

ABSTRACT: Density functional theory is used to determine differences in hydrogen abstraction and ammonia binding energies between two zeolites (BEA and MFI-type) and two α-quartz surfaces doped with Al, B, Sc, or Ga. One of the questions we wanted to answer is whether the fact that zeolite cages are made of a silica monolayer plays any role in their catalytic activity. We find no important difference. Doped α-quartz has acid hydroxyls such as those in zeolites; however, their density is very low, and doped quartz is not a shape selective catalyst. Therefore, the doped silica examined here is an inferior acid catalyst when compared to BEA or MFI.

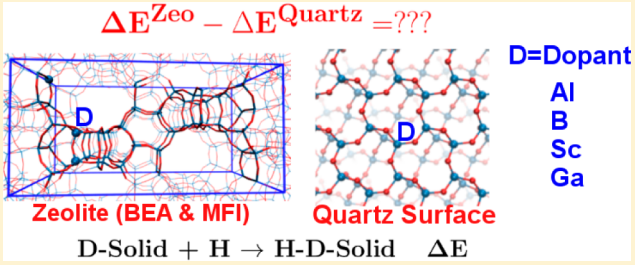

1. INTRODUCTION

Zeolites, such as doped Beta (BEA) or MFI, catalyze many useful reactions.[1−8] The structure of these zeolites consists of cages and channels made of silica "monolayers" with the silicon atoms tetrahedrally bonded to oxygen. Their chemical activity is due to doping, which is, for example, the replacement of some of the silicon atoms in the frame with trivalent atoms, such as Al, B, Ga, or Sc. One of the reasons zeolite catalysts are useful is their ability to induce size selectivity: some reactants are too large to go inside the zeolite (where catalysis takes place), some large molecules cannot be formed inside the zeolite because the cages are too small, some molecules produced inside a cage are too large to pass through the channels and exit the interior of the zeolite, whereas smaller ones can leave, thus forcing the system to produce only smaller molecules. These beneficial effects are caused by the zeolite's channel-and-cage structure. However, it is also possible that doped zeolites are different from doped silica because they consist of silica "monolayers". In this article, we use density functional theory to investigate the difference in chemical properties between the zeolites Beta and MFI and the surface of bulk silica. Those two zeolites were chosen because of their practical importance and also because the size of their unit cell is small enough to allow the performance of periodic DFT calculations. The main question is whether the chemistry of a silica monolayer in a doped zeolite is different from the chemistry of the surface of a doped slab of silica. To answer this question, we have calculated the spin density on the oxygen atoms surrounding the dopant, the strength of the H−O bond where O is an oxygen atom bonded to the dopant, and the bond of NH_3 to a hydroxyl formed near the dopant.

There are many kinds of amorphous silica[9] whose surface structure is unknown. For this reason, we compare doped Beta and MFI with doped single-crystal quartz, whose surface structure is well-characterized. The surface of quartz is normally hydroxylated, but in the present study, we examine dry quartz because this is more appropriate for comparing to a zeolite that is hydroxylated only in the neighborhood of the trivalent dopant.

We dope the zeolite by replacing one Si atom in the frame with Al, B, Ga, or Sc, which are all trivalent elements. To study silica, we replace a silicon atom in the surface of a silica slab with one of the same dopants. We have chosen dopants that are representative of what we call lower-valence dopants (LVD).[10,11] The presence of an LVD in an irreducible oxide, such as silica or the zeolite, creates an electron deficit in the system, which shows up in the electronic structure as a hole in the valence band. Unless the material is especially prepared, this hole is "compensated" for by the adsorption of a hydrogen atom, which donates an electron to fill the hole. This compensating hydrogen atom is a Brønsted acid, a feature necessary for some of the catalytic processes for which zeolites are used. We use three descriptors to compare the chemical activity of the doped zeolites with that of doped quartz: (1) the spin density on each oxygen atoms bound to the dopant, which is a measure of the "amount of hole" on the atom, which in turn is a qualitative indication of the Lewis acidity (roughly, the higher the electron deficit, the higher the Lewis acidity); (2) the energy required to remove a hydrogen atom from a hydroxyl formed near the dopant (this is the H atom that "compensates" for the hole); (3) the binding energy of gaseous NH_3 to a hydroxyl located near a dopant to form an ammonium ion. The last two energies are descriptors of the Brønsted acidity of the H in hydroxyl. A hydrogen atom that is

Received: April 30, 2015
Revised: June 17, 2015
Published: July 2, 2015

DOI: 10.1021/acs.jpcc.5b04171
J. Phys. Chem. C 2015, 119, 16106−16114

easier to remove is more acidic; the stronger the bond of NH_3 to the hydroxyl, the stronger the hydrogen's acidity.

In section 2, we describe the models used for the two zeolites, the choice of the site where the dopant is placed, and the structures used to model the surface of bulk silica. Section 3 gives details about the procedure used in computations. Section 4 discusses calculated spin densities on the oxygen atoms neighboring a dopant. Section 5 presents the binding energies of the hydrogen atoms in the hydroxyls near the dopant. Section 6 gives the binding energy of NH_3 to the hydroxyl located near the dopant. The conclusions drawn from the calculations are summarized in section 7.

2. MODELS

We have compared some of the chemical properties of BEA and silicalite (all silica MFI) doped with Al, Sc, B, and Ga to quartz surfaces doped with the same elements. The dopants were chosen to have incomplete *d*-shells (Sc) and complete *d*-shells (Al, B, and Ga). Zeolites whose frame was doped with all of these elements have been synthesized and used in catalysis. In what follows, Al-doped BEA is denoted as Al-BEA, B-doped α-quartz as B-α-quartz, and so forth.

BEA has the space group $P4_122$ and is a porous network with two mutually perpendicular straight channels along the *a*- and *b*-axis and a sinusoidal channel along the *c*-axis. The cross section of the straight channel is 7.6 Å × 6.4 Å, whereas that of the sinusoidal channel is 5.5 Å × 5.5 Å.[12] The unit cell of BEA has 192 atoms and is shown in Figure 1, along with the T-sites

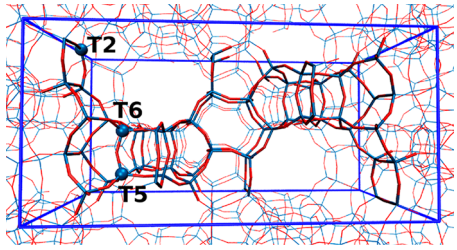

Figure 1. Crystal structure of BEA zeolite. The bold blue lines show the unit cell used in calculations. The locations of three different T sites (labeled T2, T6, and T5) are indicated by blue spheres. Si is represented by a blue vertex and O by a red one.

at which we introduced the dopants. Throughout this article, a T-site denotes a site occupied by a tetrahedrally coordinated silicon atom. When we indicate that a dopant is at a specific T-site, we mean that the dopant replaces the silicon atom that used to be located there. BEA has 9 different tetrahedral T-sites, 17 different oxygen sites,[13] and three channels, all of which have 12 T-rings (rings of 12 silicon atoms connected through oxygen atoms). We use here the nomenclature used by Bare et al.[14]

It has been shown previously that Al has no preference for a particular T-site inside the BEA framework.[15] Because it is not currently possible to study dopants located at all T-sites in the BEA framework, we have only doped the T2, T5, and T6 sites, all of which are present in the 12T channels and thus able to make contact with reactants. These sites were chosen so that they cover the whole range of NH_3 adsorption energies[15] in Al-doped BEA: T2 binds ammonia most strongly, T6 most weakly, and T5 with an intermediate binding energy.

To examine the effect of the framework-type, we have also studied the orthorhombic silicalite (MFI-type)[16,17] doped with Al, Sc, B, and Ga. Silicalite doped with Al is widely known as ZSM-5. The space group of silicalite is *PNMA* and its structure has a straight channel along the *b*-axis having a 5.4 Å × 5.6 Å cross-section and a sinusoidal channel along the *a*-axis of 5.1 Å × 5.4 Å cross-section. Both channels have 10 T-sites.[18] The orthorhombic crystal structure of silicalite has 12 crystallographically different T-sites and 26 crystallographically different oxygen sites. The unit cell has 288 atoms and is shown in Figure 2 along with the T-sites studied in this work. MFI has

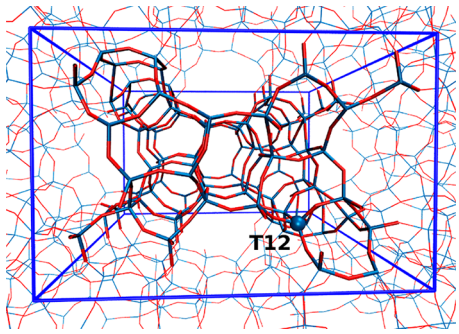

Figure 2. Crystal structure of MFI-type zeolite. The unit cell (which is the same as the cell used in the computation) is highlighted, and the T-site where the dopant was placed is shown by a blue sphere. Si atoms are represented by blue vertexes and O by a red one.

50% more atoms than BEA, and it is computationally impractical to consider doping all inequivalent T-sites. Because of this, we have only examined the effect of placing a dopant at the T12 site. This is a catalytically relevant site placed at the cross-section of the two channels.[19]

To compare silica to BEA and silicalite, we studied the (0001) and (10$\bar{1}$0) faces of α-quartz (see the Supporting Information for details on surface preparation). In the laboratory, these surface sites are passivated rapidly in the presence of moisture. If the experiments are carried out at high temperatures under ultrahigh vacuum, cleaved silica undergoes complex surface reconstruction to saturate the dangling bonds.[20−23] One can also prepare dry surfaces by heating to dehydroxylate the silanol groups.[24−26] Because the aim of this work is to compare the catalytic activity of silica surfaces with that of zeolites that are not hydroxylated (except for the hydrogen that compensates the dopant), we used in our calculations reconstructed, dry silica surfaces.

The (0001) α-quartz surface has been studied computationally[23,27,28] and experimentally.[20,21,29] Bart et al. observed a 1 × 1 pattern in low energy electron diffraction (LEED) experiments at temperatures >600 °C in ultrahigh vacuum and upon slight etching with HF.[20,30] In addition to 1 × 1 peaks, Steurer et al.[21] also observed weak 2 × 2 peaks in helium diffraction experiments, which was assigned to alternating 2 × 1 patches.[27] Our simulations found that the 2 × 1 surface is more stable by 0.03 eV per surface SiO_2 group. Because the energy difference between the two surfaces is within the DFT error, we have studied both the 1 × 1 and 2 × 1 structures.

The 1 × 1 (Figure 3a and b) and the 2 × 1 (Figure 3c and d) structures of the (0001) α-quartz have a surface layer composed of 6Θ-rings ("Θ" denotes a Si site in silica and a 6Θ-ring consists of six silicon atoms connected by oxygen atoms). The top layer is connected to the bulk by 3Θ-rings. Note that the 1 × 1 surface structure differs from the 2 × 1 one even though the top layer in both surfaces consists of 6Θ-rings. The presence of 3Θ-rings on the reconstructed (or dehydroxylated)

DOI: 10.1021/acs.jpcc.5b04171
J. Phys. Chem. C 2015, 119, 16106−16114

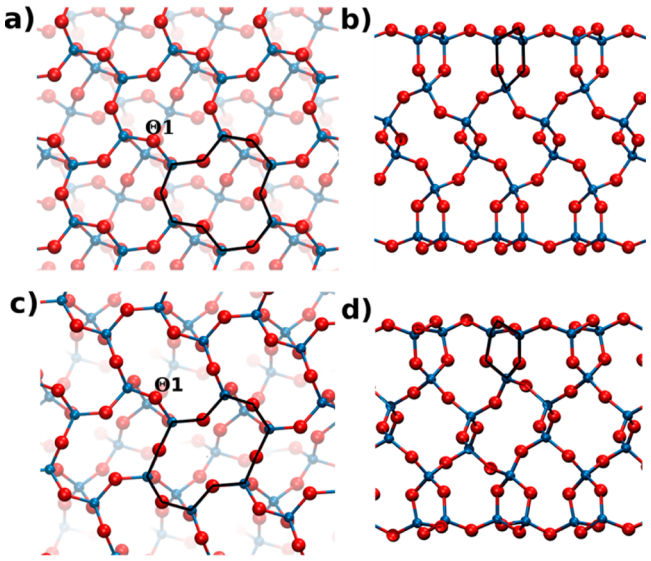

Figure 3. (a) Top view of 1 × 1 structure on a (0001) α-quartz surface. (b) Side view of 1 × 1 structure on a (0001) α-quartz surface. (c) Top view of 2 × 1 structure on a (0001) α-quartz surface. (d) Side view of 2 × 1 structure on a (0001) α-quartz surface. Si is in blue, and O is in red. The rings are highlighted by bold black lines.

silica surfaces has been observed by Raman spectroscopy,[21,30] which attributes the peak at ∼605 cm^{-1} to the ring breathing mode of 3Θ-ring. Both surfaces have *one* different Θ-site (marked in Figure 3c) and *three* different oxygens (one belonging to a 3Θ-ring) exposed to vacuum. We have studied the chemistry of all of these sites. In what follows, the (0001) α-quartz surface with 1 × 1 pattern is denoted as $(0001)_1$ quartz, and (0001) α-quartz surface with 2 × 1 pattern is denoted as $(0001)_{21}$ quartz.

The $(10\bar{1}0)$ α-quartz surface is much more complex than (0001): it has 7Θ-rings, 5Θ-rings, and 2Θ-rings (see Figure 4).

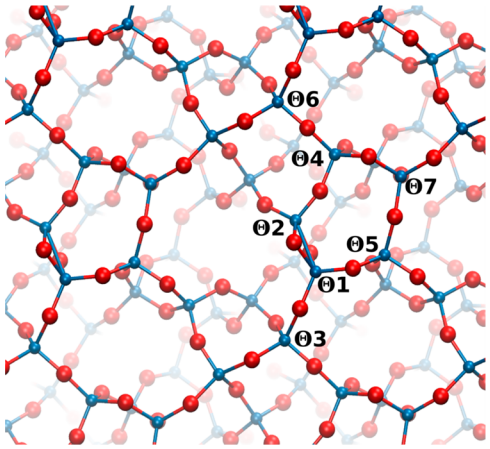

Figure 4. $(10\bar{1}0)$ α-Quartz face viewed by looking down on the surface. Si is blue, and O is red.

The presence of the 2Θ-rings is surprising considering that the O−Si−O angle in 2Θ-rings is ∼90° whereas ∼109° is the normal angle for a tetrahedral silicon. These features have been previously reported in several computational studies of dry silica surfaces.[31−36] Strained 2Θ-rings undergo rapid hydroxylation in the presence of water.[26,37] To cover a wide range of different sites on quartz surfaces, we doped seven different surface Θ-sites on the $(10\bar{1}0)$ α-quartz surface (the seven silicon sites are labeled Θ1 through Θ7 and are shown in Figure 4).

3. COMPUTATIONAL METHODOLOGY

All periodic calculations were performed using the Vienna ab initio simulation package (VASP)[38−41] with the Perdew−Burke−Ernzerhof (PBE) functional.[42] The electron−ion interactions were represented by the projector augmented-wave (PAW)[43] method with frozen-core approximation. Semicore *s* or *d* electrons were treated explicitly for Sc and Ga atoms as recommended in the literature.[44] All the other elements were treated with the default PAW pseudopotentials of VASP.

The structure of the α-quartz was obtained by starting with the XRD structure and minimizing the energy. Both the shape and the volume of the supercell were allowed to vary during geometry optimization. The plane wave basis set energy-cutoff was 500 eV. A 2 × 2 × 1, 1 × 1 × 2, and 4 × 4 × 4 Monkhorst−Pack[45] k-point grid was used for BEA, MFI, and α-quartz, respectively. The high plane wave cutoff is important because the convergence is sensitive to the finite basis set.[38,39] The optimized cell parameters are in fair agreement with the experimental values (see Table 1). The Si−O bond lengths are slightly overestimated, which is expected.[46]

Table 1. Calculated and Experimental Structural Parameters[a] of α-Quartz, All-Silica BEA, and Silicalite (MFI-Type)

structure		a (Å)	b (Å)	c (Å)	γ (deg)	<Si−O> (Å)	Si−O−Si (deg)
α-quartz	calc.	4.90	4.90	5.44	120	1.628	140
	expt.[48]	4.92	4.92	5.41	120	1.609	144
BEA	calc.	12.66	12.66	26.46	90	1.623	–
	expt.[14]	12.63	12.63	26.19	90	1.610	–
MFI	calc.	20.34	19.78	13.34	90	1.622	–
	expt.[17]	20.09	19.74	13.14	90	1.610	–

[a]Lattice parameters (*a*, *b*, *c*, and γ); geometrical parameters (average Si−O bond distances and Si−O−Si angles).

The reconstructed quartz surfaces were generated using simulated annealing[47] with the middle SiO_2 layer fixed during the runs. Brillouin zone sampling was restricted to Γ-point only, and a plane-wave energy cutoff of 350 eV was used. The self-consistency loop to determine the wave functions was terminated when the total energy change was less than 1 × 10^{-4} eV. The system was cooled from a temperature of 1500 to 500 K at a rate of 1 K per 30 fs by scaling velocities at every 150 fs. The geometry obtained by simulated annealing is further optimized by a conjugate-gradient method that is converged when the largest force on an atom was <0.02 eV/ Å.

Production runs were performed using a 400 eV cutoff. For zeolites, the Brillouin zone sampling was restricted to Γ-point only; for the (0001) α-quartz slab, the Brillouin zone sampling was done with 2 × 2 × 1 Γ-centered k-points, and for the $(10\bar{1}0)$ α-quartz slab, the Brillouin zone sampling was done with 1 × 2 × 2 Γ-centered k-points. The self-consistent loop was terminated when the total energy change was less than 5 × 10^{-6} eV. van der Waals forces were accounted for by using the Grimme's D2 method.[49] Spin-polarized calculations were performed only when the system had an unpaired electron.

DOI: 10.1021/acs.jpcc.5b04171
J. Phys. Chem. C 2015, 119, 16106−16114

Table 2. Net Spin on the Oxygen Atoms Bonded to a Dopant[a]

		Al-doped				B-doped				Ga-doped				Sc-doped			
structure		O(1)	O(2)	O(3)	O(4)	O(1)	O(2)	O(3)	O(4)	O(1)	O(2)	O(3)	O(4)	O(1)	O(2)	O(3)	O(4)
BEA	T2	0.21	0.13	0.13	0.17	0.08	0.24	0.21	0.28	0.20	0.14	0.12	0.18	0.20	0.17	0.14	0.20
	T5	0.15	0.17	0.16	0.16	0.23	0.18	0.13	0.23	0.18	0.16	0.11	0.19	0.18	0.18	0.13	0.18
	T6	0.13	0.18	0.15	0.17	0.21	0.20	0.19	0.17	0.17	0.17	0.17	0.12	0.17	0.19	0.19	0.13
MFI	T12	0.17	0.15	0.11	0.21	0.20	0.21	0.11	0.25	0.13	0.19	0.12	0.20	0.17	0.16	0.13	0.20
$(0001)_1$ quartz	Θ1−3	0.06	0.23	0.37	0.05	0.17	0.24	0.35	0.08	0.20	0.05	0.31	0.09	0.01	0.42	0.46	0.00
$(0001)_{21}$ quartz	Θ1−3	0.18	0.10	0.18	0.19	0.18	0.17	0.22	0.20	0.20	0.06	0.20	0.20	0.35	0.06	0.30	0.10
$(10\bar{1}0)$ quartz	Θ1−2	0.49	0.00	0.49	0.00	0.48	0.01	0.47	0.00	0.50	0.00	0.49	0.00	0.50	0.00	0.48	0.01
	Θ2−2	0.48	0.00	0.50	0.00	–	–	–	–	–	–	–	–	–	–	–	–
	Θ3−4	0.08	0.23	0.07	0.07	0.00	0.87	0.00	0.00	0.08	0.23	0.09	0.04	0.06	0.31	0.07	0.03
	Θ4−3	0.14	0.17	0.20	0.05	–	–	–	–	–	–	–	–	–	–	–	–
	Θ5−3	0.32	0.03	0.28	0.05	–	–	–	–	–	–	–	–	–	–	–	–
	Θ6−4	0.08	0.19	0.11	0.14	0.02	0.30	0.08	0.30	0.11	0.21	0.11	0.10	0.16	0.14	0.11	0.13
	Θ7−3	0.09	0.13	0.19	0.16	0.88	0.00	0.00	0.00	0.07	0.10	0.22	0.20	0.16	0.10	0.17	0.19

[a]The sites are defined in Figure 1 for BEA, in Figure 2 for silicalite, in Figure 3a for the 1 × 1 structure on a (0001) α-quartz surface, in Figure 3c for the 2 × 1 structure of the (0001) α-quartz surface, and in Figure 4 for the $(10\bar{1}0)$ α-quartz surface. We modified the notation to indicate the smallest ring in which the dopant is located (a Si atom is part of several rings). For example, Θ1−2 indicates the silicon labeled Θ1 (in Figure 4) is in a ring containing two silicon atoms. Θ1−2 and Θ2−2 sites are part of a 2-Θ ring connected by O(1) and O(3) oxygen atoms (see Supporting Information Figure S2). O(1)−Θ1−O(3) or O(1)−Θ2−O(3) angles are ∼90° relative to ∼109° for a SiO_4 tetrahedron.

The energies of gas-phase H_2 and NH_3 were computed using a cubic cell of length 15 Å. No change in energy was observed upon increasing the box length to 20 Å.

The Bader volume[50] was calculated using the grid-based algorithm developed by Henkelman et al.[51] The Bader charge on each atom was computed by subtracting the PAW explicit electrons from the integrated electron density inside the Bader volume. The Bader charge does not include the charge of the core. For example, a Bader charge of 0.69 on H means that H transfers 0.69 electrons to form a bond; a Bader charge of −1.59 on O means that O gains 1.59 electrons. The spin density on a particular atom was calculated by integrating the difference between spin-up and spin-down densities inside the Bader volume

$$\int_{B_V} (\rho_\uparrow - \rho_\downarrow)\, \mathrm{d}V \tag{1}$$

where the integral is over the Bader volume B_V of the atom, $\rho_\uparrow$ is the spin-up density, and $\rho_\downarrow$ is the spin-down density.

Silicas (including siliceous zeolites) are composed of SiO_4 tetrahedral units, which are very stable and have low catalytic activity. However, replacing some of the Si atoms in the frame with trivalent atoms, such as Al, Ga, or B, makes them catalytically active. Replacing a tetravalent atom with a trivalent one creates an electron deficit in the doped oxide (or zeolite). In the electronic structure, such doping creates a hole in the valence band. The presence of this hole makes the oxide or the zeolite a Lewis acid, which will react readily with a Lewis base, such as a hydrogen atom.[10,11] The practical consequence of this is that an oxygen atom in the neighborhood of the dopant will adsorb a hydrogen atom more readily than any oxygen atom in the undoped system. Borrowing from the language used when discussing doped semiconductors, one says that the absorption of H compensates the hole created by the presence of the dopant.[52] It is this hydrogen that is the Brønsted acid in doped zeolites and presumably in doped α-quartz. In practice, Brønsted acid catalysis happens by abstraction of proton by an acceptor base or in the presence of a solvent. If we compare the same process of proton transfer, it is reasonable to assume that the magnitude of electrostatic effects will cancel out while comparing qualitative trends.

The location of the hole created by doping with an LVD has been subject of extensive discussion in the literature in the case of Al-doped silica. GGA-DFT calculations predict that the hole is delocalized over the four neighboring oxygen atoms.[53,54] EPR measurements on Al-doped α-quartz have shown the hole created by the presence of substitutional Al is localized on one of the oxygen atoms as long as the temperature is below 170 K. Above this temperature, the hole is delocalized over the four oxygen atoms bonded to Al. The barrier for the motion of the hole from one oxygen to another was estimated to be ∼0.03 eV.[55] It is important to realize that when Al-doped α-quartz is made, the presence of Al is compensated by a Li or a H atom and that Al should be thought of as forming AlO_4H or AlO_4Li, not AlO_4h, where h is a hole. To prepare AlO_4h, one has to either heat AlO_4H for a long time at high temperatures (∼1000 °C) or use other drastic methods to remove H or Li.[56,57] Therefore, we assume, as argued before,[10] that at the temperatures relevant to catalysis, errors due to the delocalization of the hole are irrelevant. Moreover, we are interested in the reactivity of the hydrogen in AlO_4H in which case the hole created by Al is filled when H binds.

4. EFFECT OF THE DOPANT ON NEIGHBORING OXYGEN ATOMS

The presence of a lower-valence dopant creates an electron deficit on the surrounding oxygen atoms that we examine by calculating the Bader spin-density, which is essentially a measure of the absence of electrons (compared to the undoped system), and the Bader charge, which is the difference between the charge on an oxygen atom in the solid (zeolite or quartz) and the charge on the atom alone in vacuum. In the undoped system, the spin-density (defined by the integral in eq 1) is zero, but it differs from zero in doped oxides or zeolites because of the disruption caused by the presence of the dopant. The hole created by the dopant will be compensated for by a

DOI: 10.1021/acs.jpcc.5b04171
J. Phys. Chem. C 2015, 119, 16106−16114

hydrogen atom, which we assume is likely to bind to the oxygen atoms most depleted of electrons. Furthermore, we assume that the more depleted the oxygen atom, the more strongly it will bind the hydrogen and therefore the less acidic the hydrogen will be. These are qualitative rules, and they are not useful when we compare the binding energy of H to oxygen atoms whose spin densities are close to each other. The extent to which the rules are valid is tested in section 5, where we calculate the energy to remove H from a hydroxyl located near a dopant.

The results of the spin-density calculations are given in Table 2. We also provide Bader charges on the oxygen atoms in the undoped silica and the difference in Bader charges on the oxygen atoms of the doped silica to that of the undoped silica (see Supporting Information Tables S2 and S3). Although uniformity reigns in the case of zeolites, there are substantial differences in the spin-density on the oxygens surrounding the dopant when we change the dopant or its location. This is not surprising because the quartz surface has much higher diversity in the bonding pattern than that of the zeolites. In quartz, as in the zeolites, the silicon atom always makes four bonds with oxygen atoms. However, in both zeolites and quartz, there are rings formed from −Si−O− units, and the rings present in the two materials are different. The smallest ring in Beta or MFI has 4 Si atoms, whereas various quartz surfaces have rings containing two, three, or four silicon atoms. When a dopant replaces a silicon atom that is part of a small ring, the strain in the ring is likely to affect the spin density in the neighboring oxygen atoms, which it indeed does. To see this, in Table 2 we review the notation for the dopant position. For example, for the quartz $(10\bar{1}0)$, Θ1−2 indicates that the data is for a dopant replacing the silicon Θ1 whose location in the surface is shown in Figure 4. The number "2" in Θ1−2 tells us that this silicon is present in a ring that has two Si atoms. A Si atom is often part of several rings, and this notation specifies the smallest ring in which a dopant (replacing a Si atom) is located. The ring is strained because of the unusual angle formed by the oxygen atoms in the O−Si−O group, and this is reflected in the spin density of the oxygen atoms near the dopant: two have a strong deficit of electrons (the spin-density is 0.49), and the other two oxygens are unaffected by the presence of the dopant. If we look at the results for dopants belonging to larger rings and the difference between the oxygens surrounding the dopant, we see that there is not a dramatic difference between quartz and the zeolites, nor is there a dramatic difference between the effect of different dopants in the same host. An exception is boron, located at Θ3−4 and Θ7−3, for which the spin-density is located essentially on one oxygen atom. This happens because boron is not bonded with that particular oxygen; whereas all dopants manage to become tetravalent (so to speak), boron is determined to be trivalent when the dopant participates in a three-silicon ring.

5. BINDING OF H TO OXYGEN ATOMS NEIGHBORING A DOPANT

As suggested earlier, we expected hydrogen binding energies on an oxygen that neighbors a dopant to correlate with the net spin-density on that oxygen atom. Of course such a qualitative rule is useful only to differentiate between oxygen atoms whose spin-density is very different. We have investigated the binding energy of H to all four oxygen atoms surrounding a dopant, but we report here only the largest binding energy for each group of four oxygen atoms because that is where the hydroxyl will be formed. The results are given in Table 3. In the case of BEA, we find that the binding energy varies very little with the T-site where the dopant is located: the largest difference is 0.05 eV, which is smaller than the errors expected from DFT calculations. To compare the effect of each dopant, we used Al-doped BEA as a reference because it has the smallest binding energy for H (highest acidity); we examine the difference between the binding energy near a dopant and the binding energy near aluminum. For B-doped BEA, the difference is 2.79 − 2.47 = 0.32 eV. Even taking into account possible errors in DFT calculations, this is a significant difference, and we conclude that Al-doped BEA is more acidic than B-doped BEA. Ga-doped BEA binds H more strongly than Al-doped BEA by 0.24 eV. The same quantity for Sc-doped BEA is 2.63 − 2.47 = 0.16 eV. We find, therefore, the following trend in acidity: Al > Sc > Ga > B. The same trend is seen in MFI except that Ga and Sc have essentially the same acidity.

Table 3. Hydrogen Abstraction Energies ΔE_H on Doped α-Quartz, All-Silica BEA, and Silicalite[a]

		ΔE_H (eV)			
	doped sites	Al-doped	B-doped	Ga-doped	Sc-doped
BEA	T2	2.52	2.77	2.64	2.55
	T5	2.47	2.76	2.70	2.63
	T6	2.50	2.79	2.71	2.66
MFI	T12	2.46	2.84	2.67	2.65
$(0001)_1$ quartz	Θ1−3	2.76	2.61	2.69	2.81
$(0001)_{21}$ quartz	Θ1−3	2.65	3.09	2.85	2.90
$(10\bar{1}0)$ quartz	Θ1−2	2.51	3.77	2.77	2.57
	Θ2−2	2.57	–	–	–
	Θ3−4	3.29	3.17	3.47	2.66
	Θ4−3	2.41	–	–	–
	Θ5−3	2.65	–	–	–
	Θ6−4	2.41	3.76	2.56	2.51
	Θ7−3	2.87	3.20	3.13	2.57

[a]The sites are defined in Figure 1 for BEA, Figure 2 for silicalite, Figure 3a for the 1 × 1 structure on a (0001) α-quartz surface, Figure 3c for the 2 × 1 structure of the (0001) α-quartz surface, and Figure 4 for the $(10\bar{1}0)$ α-quartz surface. We modified the notation for Θ to also include the smallest ring size.

In the case of $(0001)_1$ quartz, we find that the oxygen atoms surrounding Al- or Sc-doped quartz bind H more strongly, and therefore, these systems are less acidic than the zeolites having the same dopants. However, B-doped $(0001)_1$ quartz and Ga-doped $(0001)_1$ bind hydrogen less strongly than either B-doped or Ga-doped zeolites. The hydrogen atom on $(0001)_{21}$ quartz is less acidic than those of the two zeolites for all dopants. The acidity of a hydroxyl on the surface of $(10\bar{1}0)$ quartz depends very strongly on the location of the dopant. For Al-doped $(10\bar{1}0)$ quartz, when the dopant is at the Θ4−3 or Θ6−4 site, the quartz is as acidic as BEA or MFI. Because of the large number of calculations necessary, we have not examined B-, Ga-, or Sc-doped $(10\bar{1}0)$ quartz with the same level of detail as Al-doped $(10\bar{1}0)$ quartz. We find that for Al-, Sc-, and Ga-doped $(10\bar{1}0)$ quartz, the acidity is essentially the same as that of zeolites if the dopant in quartz is located at Θ6−4. Boron-doped quartz has much lower acidity than the zeolites. The behavior of the boron-doped quartz is different from that of quartz doped with the other trivalent atoms because when we form a hydroxyl near the boron, the boron decides to become trivalent: it only binds to three oxygen atoms and the hydrogen

DOI: 10.1021/acs.jpcc.5b04171
J. Phys. Chem. C 2015, 119, 16106−16114

binds to the oxygen atom spurned by boron, making a stronger H−O bond.

We conclude that, depending on the dopant position, it is possible that the doped $(10\bar{1}0)$ quartz has hydroxyls that are as acidic as the hydroxyls in the zeolite.

6. ACIDITY BASED ON THE ENERGY OF NH_3 CHEMISORPTION AT A HYDROXYL SITE

NH_3 adsorption energies are extensively used to gauge the acidity of acid catalysts. We have studied chemisorption of NH_3 to a hydroxyl in Al-doped BEA, MFI, and the (0001) quartz surfaces. Our purpose was to determine whether the absorption energy of NH_3 correlates with the stability of the hydroxyl as determined by the energy required for removing the H atom from the hydroxyl. We expected that a hydroxyl that binds H weakly will form a stronger bond with NH_3.

NH_3 can chemisorb inside zeolites in monodentate (single H-bond), bidendate (two H-bonds), and even tridendate (three H-bonds) form.[58−61] We found that NH_3 tridentate is not formed when NH_3 is adsorbed on quartz. We confined our calculations to bidentate NH_3 states because they were found to be more prevalent in the previous calculations.[15]

Figure 5 shows chemisorbed NH_3 in the bidendate form in a BEA zeolite with the T6 site doped with Al. The Bader charge

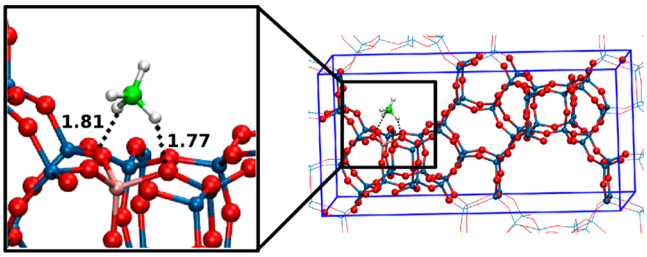

Figure 5. Optimized structure of chemisorbed ammonia inside BEA, forming a bidendate complex with the T6 site doped with Al. Si is represented by blue, O by red, H by white, and N by green.

on NH_4 is 0.87, suggesting that this group is an ammonium ion. Two of the hydrogens of the NH_4 ion form short bonds (∼1.8 Å) with the framework oxygens connected to the dopant.

We computed the chemisorption energy (ΔE_{ads}) of ammonia inside zeolites and on silica surfaces using the equation

$$\Delta E_{ads} = E_{NH_4\cdots host} - (E_{host} + E_{NH_3})$$

where $E_{NH_4\cdots host}$ is the energy of the chemisorbed NH_3 inside/on the host compound, E_{host} is the energy of the host (either doped zeolite or silica surface), and E_{NH_3} is the energy of the NH_3 molecule in a vacuum.

NH_3 chemisorption energies on Al-doped BEA, MFI, and (0001) quartz surfaces are given in Table 4. The computed chemisorption energies in BEA are in the range of 1.32−1.36 eV, whereas experiments report 1.32−1.38 eV.[62,63] The calculated chemisorption energy for the T12 site in the ZSM-5 framework is 1.56 eV, whereas the experiments report it to be in the range of 1.5−1.56 eV.[15,64−66] Binding energy measurements are limited by uncertainty caused by readsorption and diffusion inside the zeolite framework and the existence of a distribution of different acidic sites in a given zeolite. Therefore, the close agreement between the calculated and measured binding energies is probably fortuitous.

Table 4. NH_3 Chemisorption Energies (ΔE_{ads}) on (H-Al-) BEA, MFI, and (0001) α-Quartz Surfaces[a]

	Al-doped sites	ΔE_{ads} (eV)
BEA	T2	−1.35
	T5	−1.36
	T6	−1.32
MFI	T12	−1.56
$(0001)_1$ quartz	Θ1−3	−1.12
$(0001)_{21}$ quartz	Θ1−3	−1.17

[a]The sites are defined in Figure 1 for BEA, Figure 2 for silicalite, Figure 3a for the 1 × 1 structure of the (0001) α-quartz surface, and Figure 3c for the 2 × 1 structure of the (0001) α-quartz surface. We give only the value for the most strongly adsorbed bidentate NH_3 state. We modified the notation for Θ to also include the smallest ring size.

The results shown in Table 3 suggest that the acidity varies in the order Al-MFI > Al-BEA > Al-(0001)-quartz, suggesting that Al-MFI has the strongest acidic site and that Al-$(0001)_1$-quartz is the weakest acid. Comparing Tables 3 and 4, we find NH_3 chemisorption follows the same qualitative trend in acidity as indicated by H-abstraction energies; that is, Al-MFI is the strongest acid as it has the lowest H-abstraction energies, and Al-$(0001)_1$-quartz is the weakest acid as it has the highest H-abstraction energies. There are, however, quantitative differences: H-abstraction energies suggest Al-MFI has nearly the same acidity as Al-BEA ($\Delta\Delta E_H \approx 0.01$ eV), whereas NH_3 chemisorption energies suggest that Al-MFI is a much stronger acid than Al-BEA ($\Delta\Delta E_{ads} \approx 0.2$ eV). We note that this difference is within the DFT error of 0.2 eV. Alternatively, this difference could also be because of steric effects. NH_4^+ is a bigger molecule than H, and its hydrogens may interact with the oxygen atoms in the frame. The pores of BEA (6.6 Å × 6.7 Å) are larger than those of MFI (5.1 Å × 5.6 Å), and because MFI has a smaller pore, one would expect greater stabilization of the NH_4^+ ion due to the interaction described above. Therefore, one would expect higher adsorption energies, which were found in our calculations. At this point, it is not clear whether this difference is due to errors in DFT or to the fact that predictions of acidity based on H binding energy are slightly different than those based on ammonia binding energies.

7. SUMMARY

The majority of zeolites consist of monolayers of doped silica wrapped to make a three-dimensional structure with channels and pores. Doping the frame by replacing a fraction of the Si atoms in the frame with other atoms converts chemically inert zeolites into useful catalysts. The main question addressed here is whether the fact that the walls of the cages and the channels in the zeolite consist of doped silica *monolayers* is an important factor in their catalytic activity. One way to answer this question is to compare some chemistry taking place on the inner surface of a zeolite to the same chemistry on the surface of silica. We have chosen two faces of crystalline quartz as representative of silica because these surfaces have a known structure, and all silicon atoms are tetrahedrally coordinated as they are in zeolites. Many doped zeolites function as catalysts because they have a Brønsted-acid hydroxyl group next to the dopant. Therefore, we have calculated the energy needed to remove the H atom from this hydroxyl as a proxy for the hydroxyl's acidity: if removal of H requires higher energy, the

DOI: 10.1021/acs.jpcc.5b04171
J. Phys. Chem. C 2015, 119, 16106−16114

hydroxyl is less acidic. A more common measure of acidity examines the energy liberated when ammonia reacts with the hydroxyl to make an ammonium ion. We have performed a few such calculations to convince ourselves that the ammonium formation test is consistent with the test based on H bond energy in the hydroxyl. We compared zeolites doped with Al, Ga, B, and Sc because they are all trivalent dopants that act by creating an electron deficit in their surroundings, which is compensated by binding a H atom on one of the neighboring oxygen atoms. In the electronic structure, this deficit corresponds to a hole in the valence band. By evaluating the spin-density on each oxygen neighboring the dopant, we can determine how the hole is distributed amongst them. We assumed that a high hole-density on an oxygen atom indicates an atom that will bind H strongly and therefore a dopant that will make a less acidic hydroxyl. This criterion is qualitatively as good as the binding energy of H in the hydroxyl or the binding of NH_3 to the hydroxyl. The effect of the dopant depends on its position in the structure, and we have examined a variety of doping sites. For the two zeolites examined here, BEA and MFI, the location of the dopant does not make much difference as far as the acidity of the hydroxyl is concerned. For quartz, the difference can be substantial, and we have identified several dopant sites that produce very acidic hydroxyls. Therefore, it is possible to produce, on the surface of doped quartz, hydroxyls that are as acidic as those found in BEA and MFI. These calculations answer the main question we posed: we could not identify any special feature in zeolites that originates from the fact that the walls of the cages and channels are silica monolayers. Unlike other monolayers (e.g., graphene or various exfoliated oxides[67]), the doped silica monolayers that form the frame of the zeolites examined here are not much different from quartz surfaces as far as their ability to have acidic sites. This means that doped quartz is under a severe handicap as an acid catalyst. First, its area per gram is much lower than that of any zeolite. Second, there is no method of preparation of doped quartz that would guarantee that the dopants are at the surface. Third, whereas quartz has sites of comparable acidity to those in zeolites, its surface density is very low. Fourth, the absence of channels means a loss of shape selectivity, which is often one of the main reasons for using zeolite catalysts.

■ ASSOCIATED CONTENT

Supporting Information

Quartz surface preparation; pictorial representation of the numbering scheme of oxygen atoms in 2-Θ rings; Bader charges on oxygen atoms in undoped silica; and difference in Bader charges on the oxygen atoms bonded to a dopant to that of when it is not doped. The Supporting Information is available free of charge on the ACS Publications website at DOI: 10.1021/acs.jpcc.5b04171.

■ AUTHOR INFORMATION

Corresponding Author

*Telephone: 805-893-2256. Fax: 805-893-4120. E-mail: metiu@chem.ucsb.edu.

Notes

The authors declare no competing financial interest.

■ ACKNOWLEDGMENTS

We thank Dr. Henrik Kristoffersen, Dr. Ru-fen Liu, Dr. Greg Mills, and Dr. Steeve Chrétien for helpful discussions. Financial support was provided by the Department of Energy, Office of Science, Office of Basic Energy Sciences DE-FG03-89ER14048 and the Air Force Office of Scientific Research FA9550-12-1-0147. We acknowledge support from the Center for Scientific Computing at the California NanoSystems Institute and the UCSB Materials Research Laboratory (NSF MRSEC, DMR-1121053) funded in part by NSF CNS-0960316 and Hewlett-Packard. Use of the Center for Nanoscale Materials was supported by the U.S. Department of Energy, Office of Science, Office of Basic Energy Sciences, under Contract DE-AC02-06CH11357.

■ REFERENCES

(1) Auerbach, S. M.; Carrado, K. A.; Dutta, P. K. *Handbook of Zeolite Science and Technology*; Marcel Dekker, Inc.: New York, 2003.
(2) Chang, C.-C.; Green, S. K.; Williams, C. L.; Dauenhauer, P. J.; Fan, W. Ultra-Selective Cycloaddition of Dimethylfuran for Renewable *p*-Xylene with H-BEA. *Green Chem.* **2014**, *16*, 585−588.
(3) Corma, A.; Nemeth, L. T.; Renz, M.; Valencia, S. Sn-Zeolite Beta as a Heterogeneous Chemoselective Catalyst for Baeyer-Villiger Oxidations. *Nature* **2001**, *412*, 423−425.
(4) Costa, B. O. D.; Querini, C. A. Isobutane Alkylation with Solid Catalysts Based on Beta Zeolite. *Appl. Catal., A* **2010**, *385*, 144−152.
(5) Lezcano-González, I.; Boronat, M.; Blasco, T. Investigation on the Beckmann Rearrangement Reaction Catalyzed by Porous Solids: MAS NMR and Theoretical Calculations. *Solid State Nucl. Magn. Reson.* **2009**, *35*, 120−129.
(6) Maheria, K. C.; Kozinski, J.; Dalai, A. Esterification of Levulinic Acid to *n*-Butyl Levulinate Over Various Acidic Zeolites. *Catal. Lett.* **2013**, *143*, 1220−1225.
(7) Sartori, G.; Maggi, R. Use of Solid Catalysts in Friedel−Crafts Acylation Reactions. *Chem. Rev.* **2006**, *106*, 1077−1104.
(8) Corma, A.; Martínez, A. Zeolites in Refining and Petrochemistry. *Stud. Surf. Sci. Catal.* **2005**, *157*, 337−366.
(9) Waddell, W. H., Silica, Amorphous. In *Kirk-Othmer Encyclopedia of Chemical Technology*; John Wiley & Sons, Inc., 2000.
(10) McFarland, E. W.; Metiu, H. Catalysis by Doped Oxides. *Chem. Rev.* **2013**, *113*, 4391−4427.
(11) Metiu, H.; Chrétien, S.; Hu, Z.; Li, B.; Sun, X. Chemistry of Lewis Acid-Base Pairs on Oxide Surfaces. *J. Phys. Chem. C* **2012**, *116*, 10439−10450.
(12) Bare, S. R.; Kelly, S. D.; Sinkler, W.; Low, J. J.; Modica, F. S.; Valencia, S.; Corma, A.; Nemeth, L. T. Uniform Catalytic Site in Sn-Beta-Zeolite Determined Using X-Rray Absorption Fine Structure. *J. Am. Chem. Soc.* **2005**, *127*, 12924−12932.
(13) Fyfe, C. A.; Strobl, H.; Kokotailo, G. T.; Pasztor, C. T.; Barlow, G. E.; Bradley, S. Correlations Between Lattice Structures of Zeolites and Their ^{29}Si MAS NMR Spectra: Zeolites KZ-2, ZSM-12, and Beta. *Zeolites* **1988**, *8*, 132−136.
(14) Newsam, J. M.; Treacy, M. M. J.; Koetsier, W. T.; De Gruyter, C. B. Structural Characterization of Zeolite Beta. *Proc. R. Soc. London, Ser. A* **1988**, *420*, 375−405.
(15) Katada, N.; Tamagawa, H.; Niwa, M. Quantitative Analysis of Acidic OH Groups in Zeolite by Ammonia IRMS-TPD and DFT: Application to BEA. *Catal. Today* **2014**, *226*, 37−46.
(16) Flanigen, E. M.; Bennett, J. M.; Grose, R. W.; Cohen, J. P.; Patton, R. L.; Kirchner, R. M.; Smith, J. V. Silicalite, A New Hydrophobic Crystalline Silica Molecular Sieve. *Nature* **1978**, *271*, 512−516.
(17) van Koningsveld, H.; Janisen, J. C.; van Bekkum, H. The Monoclinic Framework Structure of Zeolite H-ZSM-5. Comparison with the Orthorhombic Framework of As-Synthesized ZSM-5. *Zeolites* **1990**, *10*, 235−242.
(18) Fyfe, C. A.; Gobbi, G. C.; Klinowski, J.; Thomas, J. M.; Ramdas, S. Resolving Crystallographically Distinct Tetrahedral Sites in Silicalite and ZSM-5 by Solid-State NMR. *Nature* **1982**, *296*, 530−533.
(19) Joshi, Y. V.; Thomson, K. T. Brønsted Acid Catalyzed Cyclization of C7 and C8 Dienes in HZSM-5: A Hybrid QM/MM

DOI: 10.1021/acs.jpcc.5b04171
J. Phys. Chem. C 2015, 119, 16106−16114

Study and Comparison with C6 Diene Cyclization. *J. Phys. Chem. C* **2008**, *112*, 12825−12833.
(20) Bart, F.; Gautier, M. A LEED Study of the (0001) α-Quartz Surface Reconstruction. *Surf. Sci.* **1994**, *311*, L671−L676.
(21) Steurer, W.; Apfolter, A.; Koch, M.; Sarlat, T.; Søndergård, E.; Ernst, W. E.; Holst, B. The Structure of the α-Quartz (0001) Surface Investigated Using Helium Atom Scattering and Atomic Force Microscopy. *Surf. Sci.* **2007**, *601*, 4407−4411.
(22) Murashov, V. V. Reconstruction of Pristine and Hydrolyzed Quartz Surfaces. *J. Phys. Chem. B* **2005**, *109*, 4144−4151.
(23) Rignanese, G.-M.; De Vita, A.; Charlier, J.-C.; Gonze, X.; Car, R. First-Principles Molecular-Dynamics Study of the (0001) α-Quartz Surface. *Phys. Rev. B* **2000**, *61*, 13250−13255.
(24) D'Souza, A. S.; Pantano, C. G. Mechanisms for Silanol Formation on Amorphous Silica Fracture Surfaces. *J. Am. Ceram. Soc.* **1999**, *93*, 1289−1293.
(25) Brinker, C. J.; Brow, R. K.; Tallant, D. R.; Kirkpatrick, R. J. Surface Structure and Chemistry of High Surface Area Silica Gels. *J. Non-Cryst. Solids* **1990**, *120*, 26−33.
(26) Bunker, B. C.; Haaland, D. M.; Michalske, T. A.; Smith, W. L. Kinetics of Dissociative Chemisorption on Strained Edge-Shared Surface Defects on Dehydroxylated Silica. *Surf. Sci.* **1989**, *222*, 95−118.
(27) Chen, Y.-W.; Cao, C.; Cheng, H.-P. Finding Stable α-Quartz (0001) Surface Structures via Simulations. *Appl. Phys. Lett.* **2008**, *93*, 181911.
(28) Norman, P.; Schwartzentruber, T. E.; Leverentz, H.; Luo, S.; Meana-Pañeda, R.; Paukku, Y.; Truhlar, D. G. The Structure of Silica Surfaces Exposed to Atomic Oxygen. *J. Phys. Chem. C* **2013**, *117*, 9311−9321.
(29) Jánossy, I.; Menyhárd, M. LEED Study of Quartz Crystals. *Surf. Sci.* **1971**, *25*, 647−649.
(30) Bart, F.; Gautier, M.; Duraud, J. P.; Henriot, M. $(01\bar{1}0)$ α-Quartz Surface: a LEED, XANES and ELS Study. *Surf. Sci.* **1992**, *274*, 317−328.
(31) Ceresoli, D.; Bernasconi, M.; Iarlori, S.; Parrinello, M.; Tosatti, E. Two-Membered Silicon Rings on the Dehydroxylated Surface of Silica. *Phys. Rev. Lett.* **2000**, *84*, 3887−3890.
(32) Rozanska, X.; Delbecq, F.; Sautet, P. Reconstruction and Stability of β-Cristobalite 001, 101, and 111 Surfaces During Dehydroxylation. *Phys. Chem. Chem. Phys.* **2010**, *12*, 14930−14940.
(33) Murashov, V. Ab Initio Cluster Calculations of Silica Surface Sites. *J. Mol. Struct.* **2003**, *650*, 141−157.
(34) Murashov, V. V.; Demchuk, E. Surface sites and unrelaxed surface energies of tetrahedral silica polymorphs and silicate. *Surf. Sci.* **2005**, *595*, 6−19.
(35) Koudriachova, M. V.; Beckers, J. V. L; de Leeuw, S. W. Computer Simulation of the Quartz Surface: A Combined Ab Initio and Empirical Potential Approach. *Comput. Mater. Sci.* **2001**, *20*, 381−386.
(36) Lopes, P. E. M.; Demchuk, E.; Mackerell, A. D. Reconstruction of the (011) Surface on α-Quartz: A Semiclassical Ab Initio Molecular Dynamics Study. *Int. J. Quantum Chem.* **2009**, *109*, 50−64.
(37) Bunker, B. C.; Haaland, D. M.; Ward, K. J.; Michalske, T. A.; Smith, W. L.; Binkley, J. S.; Melius, C. F.; Balfe, C. A. Infrared Spectra of Edge-Shared Silicate Tetrahedra. *Surf. Sci.* **1989**, *210*, 406−428.
(38) Kresse, G.; Furthmüller, J. Efficient Iterative Schemes for Ab Initio Total-Energy Calculations Using a Plane-Wave Basis Set. *Phys. Rev. B* **1996**, *54*, 11169−11186.
(39) Kresse, G.; Furthmüller, J. Efficiency of Ab-Initio Total Energy Calculations for Metals and Semiconductors Using a Plane-Wave Basis Set. *Comput. Mater. Sci.* **1996**, *6*, 15−50.
(40) Kresse, G.; Hafner, J. Ab Initio Molecular Dynamics for Liquid Metals. *Phys. Rev. B* **1993**, *47*, 558−561.
(41) Kresse, G.; Hafner, J. Ab Initio Molecular-Dynamics Simulation of the Liquid-Metal−Amorphous-Semiconductor Transition in Germanium. *Phys. Rev. B* **1994**, *49*, 14251−14269.
(42) Perdew, J. P.; Burke, K.; Ernzerhof, M. Generalized Gradient Approximation Made Simple. *Phys. Rev. Lett.* **1996**, *77*, 3865−3868.
(43) Blöchl, P. E. Projector Augmented-Wave Method. *Phys. Rev. B* **1994**, *50*, 17953−17979.
(44) Jain, A.; Hautier, G.; Moore, C. J.; Ping Ong, S.; Fischer, C. C.; Mueller, T.; Persson, K. A.; Ceder, G. A High-Throughput Infrastructure for Density Functional Theory Calculations. *Comput. Mater. Sci.* **2011**, *50*, 2295−2310.
(45) Monkhorst, H. J.; Pack, J. D. Special Points For Brillouin-Zone Integrations. *Phys. Rev. B* **1976**, *13*, 5188−5192.
(46) Xu, X.; Goddard, W. A. The Extended Perdew−Burke−Ernzerhof Functional with Improved Accuracy for Thermodynamic and Electronic Properties of Molecular Systems. *J. Chem. Phys.* **2004**, *121*, 4068−4082.
(47) Frenkel, D.; Smit, B. *Understanding Molecular Simulation: From Algorithms to Applications*; Academic Press Inc.: San Diego, CA, 2002.
(48) Levien, L.; Prewitt, C. T.; Weidner, D. J. Structure and Elastic Properties of Quartz at Pressure. *Am. Mineral.* **1980**, *65*, 920−930.
(49) Grimme, S. Semiempirical GGA-type Density Functional Constructed With a Long-Range Dispersion Correction. *J. Comput. Chem.* **2006**, *27*, 1787−1799.
(50) Bader, R. F. W. *Atoms in Molecules: A Quantum Theory*; Oxford University Press: Oxford, UK, 1994.
(51) Henkelman, G.; Arnaldsson, A.; Jónsson, H. A Fast and Robust Algorithm for Bader Decomposition of Charge Density. *Comput. Mater. Sci.* **2006**, *36*, 354−360.
(52) Hu, Z. P.; Li, B.; Sun, X.; Metiu, H. Chemistry of Doped Oxides: The Activation of Surface Oxygen and the Chemical Compensation Effect. *J. Phys. Chem. C* **2011**, *115*, 3065−3074.
(53) Lægsgaard, J.; Stokbro, K. Hole Trapping at Al impurities in Silica: A Challenge for Density Functional Theories. *Phys. Rev. Lett.* **2001**, *86*, 2834−2837.
(54) Pacchioni, G.; Frigoli, F.; Ricci, D.; Weil, J. A. Theoretical Description of Hole Localization in a Quartz Al Center: The Importance of Exact Electron Exchange. *Phys. Rev. B* **2000**, *63*, 054102.
(55) Schnadt, R.; Schneider, J. The Electronic Structure of the Trapped-Hole Center in Smoky Quartz. *Phys. Kondens. Mater.* **1970**, *42*, 19−42.
(56) Nuttall, R. H. D.; Weil, J. A. The Magnetic Properties of the Oxygen−Hole Aluminum Centers in Crystalline SiO_2.I. $[AlO_4]^0$. *Can. J. Phys.* **1981**, *59*, 1696−1708.
(57) Halliburton, L. E.; Koumvakalis, M. E.; Martin, J. J. Radiation Effects in Crystalline SiO_2: The Role of Aluminum. *J. Appl. Phys.* **1981**, *52*, 3565−3574.
(58) Agarwal, V.; Huber, G. W.; Conner, W. C., Jr.; Auerbach, S. M. DFT Study of Nitrided Zeolites: Mechanism of Nitrogen Substitution in HY and Silicalite. *J. Catal.* **2010**, *269*, 53−63.
(59) Brändle, M.; Sauer, J. Acidity Differences Between Inorganic Solids Induced by Their Framework Structure. A Combined Quantum Mechanics/Molecular Mechanics Ab Initio Study on Zeolites. *J. Am. Chem. Soc.* **1998**, *120*, 1556−1570.
(60) Katada, N.; Suzuki, K.; Noda, T.; Sastre, G.; Niwa, M. Correlation between Brønsted Acid Strength and Local Structure in Zeolites. *J. Phys. Chem. C* **2009**, *113*, 19208−19217.
(61) Solans-Monfort, X.; Sodupe, M.; Branchadell, V.; Sauer, J.; Orlando, R.; Ugliengo, P. Adsorption of NH_3 and H_2O in Acidic Chabazite. Comparison of ONIOM Approach with Periodic Calculations. *J. Phys. Chem. B* **2005**, *109*, 3539−3545.
(62) Katada, N.; Suzuki, K.; Noda, T.; Park, M. B.; Min, H.-K.; Hong, S. B.; Niwa, M. Ammonia IRMS-TPD Characterization of Brønsted Acid Sites in Medium-pore Zeolites with Different Framework Topologies. *Top. Catal.* **2010**, *53*, 664−671.
(63) Pinto, R. R.; Borges, P.; Lemos, M. A. N. D. A.; Lemos, F.; Védrine, J. C.; Derouane, E. G.; Ribeiro, F. R. Correlating NH_3-TPD and ^{1}H MAS NMR Measurements of Zeolite Acidity: Proposal of an Acidity Scale. *Appl. Catal., A* **2005**, *284*, 39−46.
(64) Parrillo, D. J.; Gorte, R. J. Characterization of Acidity in H-ZSM-5, H-ZSM-12, H-Mordenite, and H-Y Using Microcalorimetry. *J. Phys. Chem.* **1993**, *97*, 8786−8792.

DOI: 10.1021/acs.jpcc.5b04171
J. Phys. Chem. C 2015, 119, 16106−16114

(65) Parrillo, D. J.; Gorte, R. J.; Farneth, W. E. A Calorimetric Study of Simple Bases in H-ZSM-5: A Comparison with Gas-Phase and Solution-Phase Acidities. *J. Am. Chem. Soc.* **1993**, *115*, 12441−12445.
(66) Auroux, A.; Vedrine, J. C., Microcalorimetric Characterization of Acidity and Basicity of Various Metallic Oxides. In *Catalysis by Acids and Bases*; Imelik, B., Ed.; Elsevier B.V., 1985; Vol. *20*, pp 311−318.
(67) Nicholas, J. B.; Winans, R. E.; Harrison, R. J.; Iton, L. E.; Curtiss, L. A.; Hopfinger, A. J. An Ab Initio Investigation of Disiloxane Using Extended Basis Sets and Electron Correlation. *J. Phys. Chem.* **1992**, *96*, 7958−7965.

DOI: 10.1021/acs.jpcc.5b04171
J. Phys. Chem. C 2015, 119, 16106−16114